

The Effect of Chemical Composition on High Temperature Behaviour of Fe and Cu Doped Mn-Co spinels

Masi, Andrea; Bellusci, Mariangela; McPhail, Stephen J.; Padella, Franco; Reale, Priscilla; Hong, Jong-Eun; Steinberger-Wilckens, Robert; Carlini, Maurizio

DOI:

[10.1016/j.ceramint.2016.11.135](https://doi.org/10.1016/j.ceramint.2016.11.135)

License:

Creative Commons: Attribution-NonCommercial-NoDerivs (CC BY-NC-ND)

Document Version

Peer reviewed version

Citation for published version (Harvard):

Masi, A, Bellusci, M, McPhail, SJ, Padella, F, Reale, P, Hong, J-E, Steinberger-Wilckens, R & Carlini, M 2017, 'The Effect of Chemical Composition on High Temperature Behaviour of Fe and Cu Doped Mn-Co spinels', *Ceramics International*, vol. 43, no. 2, pp. 2829-2835. <https://doi.org/10.1016/j.ceramint.2016.11.135>

[Link to publication on Research at Birmingham portal](#)

Publisher Rights Statement:

Checked 2/12/2016

General rights

Unless a licence is specified above, all rights (including copyright and moral rights) in this document are retained by the authors and/or the copyright holders. The express permission of the copyright holder must be obtained for any use of this material other than for purposes permitted by law.

- Users may freely distribute the URL that is used to identify this publication.
- Users may download and/or print one copy of the publication from the University of Birmingham research portal for the purpose of private study or non-commercial research.
- User may use extracts from the document in line with the concept of 'fair dealing' under the Copyright, Designs and Patents Act 1988 (?)
- Users may not further distribute the material nor use it for the purposes of commercial gain.

Where a licence is displayed above, please note the terms and conditions of the licence govern your use of this document.

When citing, please reference the published version.

Take down policy

While the University of Birmingham exercises care and attention in making items available there are rare occasions when an item has been uploaded in error or has been deemed to be commercially or otherwise sensitive.

If you believe that this is the case for this document, please contact UBIRA@lists.bham.ac.uk providing details and we will remove access to the work immediately and investigate.

The Effect of Chemical Composition on High Temperature Behaviour of Fe and Cu Doped Mn-Co spinels

Andrea Masi ^{a,b,c}, Mariangela Bellusci ^a, Stephen J. McPhail ^a, Franco Padella ^a, Priscilla Reale ^a, Jong-Eun Hong ^{b,1}, Robert Steinberger-Wilckens ^b, Maurizio Carlini ^c

^a) ENEA C.R. Casaccia, 00123 Rome, Italy

^b) School of Chemical Engineering, University of Birmingham, Edgbaston, Birmingham B15 2TT, UK

^c) University of Tuscia - DAFNE, 01100 Viterbo, Italy

*Corresponding Author: Andrea Masi, tel: +393394188284, fax +39 06 30486357, mail: andrea.masi@enea.it, address: via Anguillarese 301, 00123, Roma (Italy)

¹ Current address: Fuel Cell Laboratory, Korea Institute of Energy Research, 152 Gajeon-ro, Daejeon, xxxxx, Republic of Korea

Abstract

Mixed Mn-Co spinels are currently studied as protective coating materials for Solid Oxide Fuel Cells interconnects. Compositional changes in manganese cobaltites lead to modifications in the materials properties, such as sintering behaviour, thermal expansion and electrical conductivity, with advantages in the technological application. In this work, the effect of Fe, Cu and simultaneous Fe+Cu doping of Mn-Co spinels has been studied. Different oxide powder mixtures were prepared with a High Energy Ball Milling (HEBM) treatment, obtaining highly reactive oxides that easily form single spinel phase compounds by moderate heating. The effect of the composition is observed on high temperature stability of the spinel phase and on densification behaviour of the powders, greatly enhanced by copper addition.

Analyses carried out on sintered pellets allow to observe simple relations among dopant concentration, thermal expansion and electrical conductivity. The combined effect is obtained in case of the simultaneous addition of multiple dopants. An appropriate composition can be therefore designed to obtain a material characterized by enhanced sintering behaviour, high electrical conductivity and tailored thermal expansion to fulfil the application requirements.

Keywords

A. Milling B. Spinel C. Thermal expansion C. Electrical Conductivity

1. Introduction

Development and commercial breakthrough of Solid Oxide Fuel Cells (SOFCs) is necessarily linked to reduction of costs and increase of long-term reliability. One of the key-factors is represented by the substitution of ceramic interconnects with metallic parts. High chromium ferritic steels have been identified as the most promising candidate material because of their low cost and their Coefficient of Thermal Expansion (CTE) compatibility with the SOFC materials [1]. In operating conditions, however, long-term performance degradation arises due to the formation of insulating chromium-rich oxides and the evaporation of volatile Cr species, that can migrate and react with the cathode material, thereby reducing the active surface area [2]. The application of protective coating is therefore mandatory to avoid these issues, and several materials are being studied, including reactive element oxides, rare earth perovskite and spinel oxides [3,4]. Among these materials, Mn-Co spinels with Co:Mn in the 1:1÷2:1 range, characterized by high conductivity values and good thermal expansion compatibility with ferritic stainless steels, have been suggested as the best candidates.

In view of large-scale application, cheap wet-powder coating techniques, such as spray coating, screen printing and ink-jet printing, would be preferred. These methods rely on their own ink formulations and sintering thermal treatments, and the effectiveness of the coating is therefore related to efficient sintering steps. Sintering Mn-Co spinel powders in air requires high temperature (e.g. 1000°C [5]), raising concerns about the degradation of mechanical properties that could be induced in the substrate. To achieve sufficient densification at lower temperature, thermal treatments in reducing atmosphere are widely used, followed by oxidation steps to recover the spinel structure [6,7].

Alternatively, reduction of sintering temperature can be achieved with the introduction

of further elements acting as sintering aids, such as Cu and Ni [8,9], representing an attractive approach avoiding a more expensive multi-step sintering treatment.

The addition of dopant elements, such as transition metals or reactive elements like Fe, Ti, Cu, Ni or Y, has furthermore been proven effective in enhancing application related to properties such as chromium retention capability or electrical conductivity [8,10,11].

However, changes in composition affect the thermal expansion behaviour: Mn-Co spinels possess CTE values in the $9.7\div 13.5\cdot 10^{-6}\text{ K}^{-1}$ [12–15] and $10.6\div 14.1\cdot 10^{-6}\text{ K}^{-1}$ [5,8,10,16] ranges, respectively at 800°C and at 1000°C. Cu and Ni doping produces an increase in CTE [8,9,14,15,17], while Fe and Ti lower this property [10]. No clear relation between CTE and dopant concentration can be however deduced from the literature, mostly due to the high dispersion of results. Furthermore, to the best of our knowledge, no results have been reported related to the effect of simultaneous doping.

HEBM is a consolidated, cost effective and environmentally friendly powder processing technique widely applied in material science. The technique consists in the exposure of defined quantities of powder reactants to repeated energy transfer phenomena obtained by colliding balls. The kinetic energy released from the balls to the powder can induce several physico-chemical phenomena, the first being represented by fine grinding of particles, and therefore formation of new active surfaces. Nanostructuration of the powder can occur at this stage, enhancing significantly powder reactivity, followed by interdiffusion, atomic rearrangements, nucleation of stable or metastable phases, amorphization, re-crystallization phenomena and so on [18].

In our previous works, High Energy Ball Milling (HEBM) was evaluated as a synthesis route to obtain mixed spinels starting from oxide powders [19,15]. A HEBM treatment carried out on Mn-Co oxides promotes the room temperature solid state mechano-chemical reaction between Mn and Co oxide mixtures, with a unitary reaction yield

after 65 h of milling. Powders obtained after relatively short mechano-chemical treatments (e.g. 10 h), despite not containing a single phase compound, are characterized by significantly enhanced reactivity with respect to pristine oxides, and easily evolve to form the equilibrium products when subjected to moderate heating (i.e. $T < 800^{\circ}\text{C}$).

In this work, to study the effect of Fe, Cu and simultaneous Fe+Cu doping on the chemico-physical properties of Mn-Co spinels, different powder mixtures of Mn, Co, Fe and Cu oxides are prepared and subjected to a HEBM treatment. The obtained highly reactive powder samples are characterized in their thermal evolution and sintering properties, and differences on powder densification behaviour and high temperature spinel stability induced by the dopant contents are observed and reported. Finally, the effect of different metal compositions on thermal expansion and electrical conductivity of sintered samples is evaluated and discussed.

2. Experimental Procedure

Mn₃O₄ (Sigma Aldrich, 97%), Co₃O₄ (Sigma Aldrich, 99%), CuO (Carlo Erba, 99%) and Fe₂O₃ (Carlo Erba, 99%) were mixed in stoichiometric quantities to obtain the compositions reported and labelled in Table 1. The HEBM process was performed in a SPEX8000M mixer mill, using cylindrical steel vials (60 cm³ volume) and steel balls (10mm diameter) with powder to balls weight ratio of 1:10. Vials were loaded with 8g of powder, sealed in argon atmosphere and subjected to 10 hours of milling. After the milling treatment, the absence of contamination from the milling media was assessed evaluating chromium presence by means of energy-dispersive X-ray microanalysis (Hitachi TM3030Plus).

X-Ray diffraction analyses (XRD) were carried out on a 120° angular dispersion X-ray diffractometer (Italstructure, curved position sensitive detector from INEL), equipped with Fe K_{α1} radiation source. Phase identification was performed on collected patterns using the PDF-2 database [20] as reference data. Lorentzian fitting of selected reflections allowed to evaluate cell parameters and to calculate accordingly theoretical densities, considering nominal compositions of the samples.

Morphology of the samples was evaluated using N₂ adsorption at 77K technique (Quantachrome Autosorb-iQ). Specific surface area (SSA) values were obtained by applying the BET method [21]. BET particle size l was calculated as $l = \frac{6}{SSA \cdot \rho}$, where ρ is the material density.

Thermogravimetric analysis was carried out in air using a Perkin Elmer thermobalance (Pyris Diamond TG/DTA, Perkin Elmer) with the following procedure: heating scan up to 1200°C at 5°C/min, 60 minutes of isothermal step and cooling to room temperature at 5°C/min.

Dilatometric measurements were performed in a push-rod dilatometer (DIL 402 C, NETZSCH). To evaluate sintering behaviour, consolidated pellets of about 6mm diameter length were obtained by uniaxial cold pressing (3.5 T/cm²) and heated in air with a heating rate of 5°C/min up to 1200°C. Thermal expansion measurements were carried out with a heating rate of 10°C/min on pellets of about 6mm diameter and 2.5mm height sintered as described later in the text. Average CTE was calculated between room temperature and 800°C as: $CTE = \frac{1}{L_0} \frac{\Delta L}{\Delta T}$, where L_0 is the initial length and ΔL represents the length change occurring in the ΔT temperature range.

To assess electrical conductivity, pellets of about 10mm diameter were obtained by uniaxial cold pressing (3.5 T/cm²) and sintered similarly to thermal expansion samples. The conductivity was measured by applying the Van der Pauw method [22] (PAR273A

potentiostat coupled to a HP 3457A multimeter) in the 500–800°C temperature range.

Activation energy E_a was calculated from the Arrhenius plot obtained using the

formula: $\sigma = \frac{\sigma_0}{T} e^{-\frac{E_a}{kT}}$, where σ is the conductivity, T the temperature, σ_0 the pre-

exponential factor, E_a the activation energy and k the Boltzmann's constant.

3. Results and discussion

3.1. Powder characterization

The XRD patterns of the 10 hours milled powders are reported in Fig. 1. All the examined samples are characterized by similar patterns, with significant peak broadening ascribable to nanostructuration of crystallites and strain. Starting with the MnCo_{1.8}Fe_{0.2} pattern, main peaks are ascribable to the presence of a cubic spinel compound, compatible with Co₃O₄ phase (JCPDS card n. 42-1467). Peaks related to the Mn₃O₄ compound are not evident, confirming that the cobalt rich phase exhibits a high stability during the mechano-chemical treatment, as already observed in the case of similar oxides mixtures [19,15]. The asymmetry of Co₃O₄ peaks towards lower angles could be ascribed to the nucleation of a cubic spinel phase characterized by higher lattice parameter, most likely a mixed spinel similar to MnCo₂O₄ (JCPDS card n. 23-1237). The small broadened peaks at $2\theta \cong 48$ degrees is due to the presence of highly destructured Fe₂O₃ phase (JCPDS card n. 33-0664), and are more evident in the MnCo_{1.6}Fe_{0.4} pattern, as expected due to the higher iron content. In the case of copper containing samples, instead, clear evidences of CuO phase (JCPDS card n. 48-1548) are not observed, suggesting low stability of CuO structure during the HEBM treatment, most likely due to facile diffusion of small copper ions into the spinel lattice during the mechano-chemical treatment. In the MnCo_{1.6}Fe_{0.2}Cu_{0.2} pattern, similar to what is observed for MnCo_{1.8}Fe_{0.2} sample, features of a hematite phase are visible.

Therefore, as shown in the XRD analysis, the 10h HEBM treatment does not produce a single equilibrium spinel phase but some metastable mixture of metal oxides. Nitrogen adsorption measurements at 77K were carried out to calculate BET specific surface area and thus evaluate the degree of particle aggregation. The obtained values are reported in Table 2. Mn-Co-Fe samples exhibit comparable surface areas, while Cu addition seems to favour higher degrees of aggregation resulting in lower surface areas. The size of particles calculated with BET ranges between 160 and 330nm. In order to evaluate the differences in the high temperature behaviour of the powders, which is induced by the cobalt substitution, thermogravimetric analyses up to 1200°C were carried out and are reported in Fig. 2. The samples exhibit an initial weight loss, ascribable to adsorbed humidity departure. In the 200–500°C temperature range a weight gain step is instead observed. This phenomenon can be related to the powder comminution and activation induced by the HEBM, carried out in Ar atmosphere. Highly reactive new surfaces are produced during the mechano-chemical treatment that interacts with oxygen already at low temperature giving rise to the oxidation phenomena observed during the thermal treatment. Moreover, the HEBM treatment induces a high degree of interdiffusion of the precursor oxides with solid state reactions at the new interfaces, most likely with the formation of highly anion defective lattices, due to the milling atmosphere. Subsequent filling of the oxygen vacancies may therefore occur when exposed to air at moderate temperatures. The occurrence of similar weight gain phenomena and the existence of metastable non-stoichiometric mixed valence spinels has been observed for similar systems and ascribed to high reactivity due to high nanostructuration of the compounds [23], and it is supposed that similar mechanisms occur here, due to the defectivity induced by the HEBM treatment.

Regarding the influence of the composition on this weight gain step, it can be observed that the magnitude of the weight gain increases following the order: $\text{MnCo}_{1.6}\text{Fe}_{0.4} < \text{MnCo}_{1.8}\text{Fe}_{0.2} < \text{MnCo}_{1.6}\text{Fe}_{0.2}\text{Cu}_{0.2} < \text{MnCo}_{1.8}\text{Cu}_{0.2}$. This can be related to the initial powder composition: Co_3O_4 precursor is substituted with species characterized by different oxygen content (i.e. Fe_2O_3 and CuO), and it is likely to suppose that, with Fe and Cu ions presence in the spinel lattice due to the mechano-chemical treatment, the oxygen uptake of the metastable spinels will be inversely related to the initial oxygen content.

Following this weight gain step, in the 500–700°C temperature range a gradual weight loss can be observed, related to the rearrangement and homogenization of the oxidized compound to form the expected high temperature single spinel phase. At about 800°C, in fact, the curves reach a plateau, suggesting that no further oxygen release occurs.

Also in this weight change step a relationship between the weight loss and the material composition can be observed: in particular, the weight loss increases following the order: $\text{MnCo}_{1.8}\text{Cu}_{0.2} < \text{MnCo}_{1.6}\text{Fe}_{0.2}\text{Cu}_{0.2} < \text{MnCo}_{1.8}\text{Fe}_{0.2} < \text{MnCo}_{1.6}\text{Fe}_{0.4}$. The samples characterized by the higher initial oxygen content show therefore the higher mass loss.

The substitution of the $\text{Co}^{2+}/\text{Co}^{3+}$ precursor with higher or lower oxidation state species, respectively Fe^{3+} from Fe_2O_3 and Cu^{2+} from CuO , affects the oxidation behaviour of the milled powder both during the formation of the metastable spinels and during the homogenization reaction that produce equilibrium compounds. In our previous work [19], we observed that during mechano-chemical treatment of Mn and Co oxides the reaction proceeds through nucleation and growth of mixed phases rather than through interdiffusion phenomena of the starting oxides. Observing how the thermal behaviour of the doped powders is influenced by the initial composition, it is likely to suppose that

the formation of Fe and Cu doped phases occurs already during the milling step, suggesting that a similar reaction mechanism is involved.

Further increase of temperature above 1000°C leads to a third weight loss phenomenon, that can be related to metal reduction from the spinel phases with related oxygen release, due to the formation of Me(II) oxide phases. The existence of a high temperature spinel-Me^{II}O multi-phase boundary is known for Co-Mn oxide mixtures [24], and the data reported here suggest that a similar behaviour is retained with Fe and Cu addition to the spinel composition, with some differences in the onset temperature. Co substitution with Fe appears to extend the spinel stability region. Copper substitution promotes instead the spinel de-mixing at lower temperature.

During the successive cooling stage, the weight loss associated to the high temperature phase transition is recovered for all the stoichiometries, compatibly with spinel stability at intermediate temperature. In the case of the MnCo_{1.8}Cu_{0.2} sample, weight gain occurs in two steps, suggesting a multiple oxidation process that could be due to multiple high temperature dual-phase regions, as observable in the Cu-Co oxides phase diagram [25].

To evaluate sintering behaviour, consolidated pellets were formed with the 10h HEBM powders. The pre-sintering densities are reported in Table 3: similar values of density are obtained for all the different samples, as expected from the processing of morphologically similar powders. Shrinkage and shrinkage rate curves are reported in Fig. 3. Mn-Co-Fe samples show behaviour comparable to similar Mn-Co spinels [15], with sintering temperatures of about 1040–1060°C and maximum densification rates at 1150°C approximately. The addition of Cu significantly improves sintering: in the case of MnCo_{1.8}Cu_{0.2} and MnCo_{1.6}Fe_{0.2}Cu_{0.2} samples, shrinkage starts at approximately 925–950°C, with maximum densification rate occurring at $T \cong 1000^\circ\text{C}$.

XRD analysis carried out on the pellets after dilatometric measurements indicated however the presence of secondary phases: differently with respect to thermogravimetric measurements, thermal treatment of the pellets at 1200°C could result in the lack of recovery of the single spinel structure upon cooling. This is most likely due to high packing and higher crystals growth, limiting oxygen diffusion. Being crucial to obtain single phase pellets to evaluate precisely thermal expansion and electrical conductivity properties, different sintering procedures were studied to obtain dense single phase pellets. In the case of the MnCo_{1.8}Fe_{0.2} and MnCo_{1.6}Fe_{0.4} sample, requiring sintering temperature of 1200°C to achieve high density values, a lower temperature (800°C) dwell step was introduced to facilitate spinel recovery. The significantly lower sintering temperature of Cu containing compounds, as evidenced by dilatometric analysis, allowed to reduce the maximum treatment temperature to 1000°C still obtaining dense pellets.

The sintered densities obtained for the different samples, reported in Table 3, show how Cu inclusion leads to a significant enhancement of densification: Cu substituted samples are in fact characterized by higher density with respect to Mn-Co-Fe samples even with a reduction in sintering temperature of 200K.

X-Ray diffraction patterns of the sintered samples are reported in Fig. 4. All compositions exhibit a single cubic spinel phase. The evidence of well-defined peaks suggests a significant crystal growth during the sintering process. Peak shifts with respect to the standard MnCo₂O₄ phase are observed for the different compositions, highlighted by the calculated cell parameters reported in Table 4. In particular, due to the different size of dopants ionic radius with respect to the substituted cobalt [26], Fe-Co substitution promotes the enlargement of the lattice (8.27Å for MnCo₂O₄ [20]),

differently from Cu-Co substitution that, due to similar ionic radii, does not induce significant changes in the cell parameter.

3.2. Thermal expansion

Thermal expansion compatibility between the substrate and the coating material is a crucial factor to avoid mechanical stress that could arise during thermal cycles or long term operation and could promote cracking or delamination of the coatings. To evaluate CTE of the examined materials, the sintered pellets were subjected to dilatometric analyses. In Fig. 5 the expansion curves are reported, and average CTE values calculated between room temperature and 800°C are listed in Table 5. All the samples exhibit a linear behaviour through all the measured temperature range. The results here obtained are comparable to values found in literature for similar compounds (e.g. [10]). Considering the thermal expansion of ferritic stainless steels, i.e. $11\text{--}13 \cdot 10^{-6} \text{K}^{-1}$ [27], MnCo_{1.8}Cu_{0.2} samples possess lower compatibility with respect to the Fe containing samples.

To evaluate how cobalt substitution with Fe and Cu affects this property, in Fig. 6 are depicted the CTE values at 800°C versus the cobalt content for the different samples, compared with result previously obtained on a MnCo₂O₄ spinel [15]. It can be observed a clear negative trend between CTE value and iron content, while MnCo_{1.8}Cu_{0.2} sample is characterized by higher CTE value than the undoped sample. Consistently with the single metal doped samples, the combined effect is obtained in the MnCo_{1.6}Fe_{0.2}Cu_{0.2} compound, the CTE of which is ranged between those of MnCo_{1.8}Fe_{0.2} and MnCo_{1.8}Cu_{0.2}. This result suggests that the CTE of Mn-Co spinels can be tuned in the examined range by compositional tailoring, as the effect of the

cobalt substitution with copper and iron on CTE is retained with the simultaneous doping.

Regarding the dependence of the CTE with the composition, the obtained results are in agreement with previous studies that suggest the occurrence of a relation between CTE and the different occupations and valence states in the spinel lattice [28]. In particular, mixed element spinels characterized by higher valence differences among the sites possess higher CTE, especially when this difference occurs between octahedrally coordinated cations [28]. In Mn-Co spinels, tetrahedral sites are occupied preferentially by Co^{II} species, while octahedral sites are occupied by Co^{II} , Co^{III} , Mn^{III} and Mn^{IV} . The amount of Co^{II} and Mn^{IV} , strictly connected due to charge neutrality restraints, is maximum when $\text{Co}:\text{Mn}\sim 2$ [29]. The substitution of Co with Fe occurs with Fe^{III} species occupying preferentially octahedral sites in place of Co atoms [11], reducing the amount of octahedral Co^{II} and therefore the amount of species characterized by different valences. When copper is added to the compound, instead, Cu atoms tend to occupy preferentially tetrahedral sites [30], with the presence of Cu^{I} and Cu^{II} species.

Moreover, copper addition is likely to promote octahedral Mn^{III} oxidation to Mn^{IV} to maintain charge neutrality [30], increasing further the number of different valence species in the lattice and therefore CTE.

When Co is substituted by both Fe and Cu, the enhancement of CTE due to Cu^{I} and Cu^{II} introduction on tetrahedral sites is counterbalanced by the CTE decrease induced by the Fe^{III} presence in octahedral sites, and, with Fe and Cu ions not being competitors for lattice sites occupation in the examined composition range, the overall CTE change can be considered as limited to the sum of the single dopants contributions.

3.3. Electrical conductivity

Electrical conductivity was evaluated by means of Van der Pauw method in the temperature range 500–800°C. In Fig. 7 the Arrhenius plots are reported. All samples exhibit a linear relation: evaluating the slope of the linear fits to the Arrhenius curves activation energy was calculated, and results are reported in Table 6. All samples show similar values of about 0.5 eV, suggesting a similar conduction mechanism.

In Fig. 8 the conductivity values measured at 800°C for the different samples are reported as a function of the cobalt content, and compared with an undoped MnCo_2O_4 spinel [15]. It can be observed a clear decreasing trend upon the substitution of Co with Fe, with conductivity of about 51 S/cm and 36 S/cm for $\text{MnCo}_{1.8}\text{Fe}_{0.2}$ and $\text{MnCo}_{1.6}\text{Fe}_{0.4}$ samples respectively. Co substitution with Cu significantly increases conductivity, and similar enhancements are observed when cobalt is substituted in the reference material ($\text{Mn}_{1.8}\text{Co}_{1.8}\text{Cu}_{0.2}$ versus MnCo_2O_4) or in the iron doped sample ($\text{MnCo}_{1.6}\text{Fe}_{0.2}\text{Cu}_{0.2}$ versus $\text{Mn}_{1.8}\text{Co}_{1.8}\text{Fe}_{0.2}$).

The electrical conductivity in spinels is associated with a small polaron hopping mechanism between mixed valence elements on octahedral sites and in Mn-Co oxides it is related to $\text{Co}^{\text{II}}/\text{Co}^{\text{III}}$ and $\text{Mn}^{\text{III}}/\text{Mn}^{\text{IV}}$ pairs [13,28]. The valence state concentration ratio affects therefore significantly conductivity properties. The observed decrease in conductivity with Fe substitution is related to the preferential occupation of octahedral sites by Fe^{III} atoms, not involved in polaron formation, limiting the charge carrier density [11]. Regarding Cu addition, the conductivity enhancement could be due to multiple factors: the aforementioned promotion of Mn^{III} oxidation to Mn^{IV} to maintain charge neutrality [30], occurring with the presence of Cu^{I} and Cu^{II} species in the lattice, could increase the number of active pairs on octahedral sites. Furthermore, Cu atoms in tetrahedral sites could contribute indirectly through mediation of charge transfers

between close Mn atoms in octahedral sites [31]. The electrical conductivity enhancement observed with copper addition therefore could be attributed to an indirect enhancement of Mn pairs contribution.

Similarly to what was observed for CTE, most likely due to the absence of competition for lattice site occupation among the dopants, our results suggest that the effect of the simultaneous substitution is limited to the sum of the single factors.

4. Conclusions

Doped spinels were successfully produced by a mechano-chemically enhanced solid state reaction synthesis. The effect of doping has been clearly highlighted with respect to high temperature stability, sintering behaviour, CTE and electrical conductivity. Through a high energy ball milling treatment, Fe and Cu substituted Mn-Co highly reactive oxide mixtures were obtained. The powders easily form the expected single cubic phase when exposed to moderate temperature ($T < 800^{\circ}\text{C}$). Influence of the dopant content was observed on thermal stability of the spinel phase, enhanced by Fe and decreased by Cu addition.

Regarding the densification behaviour, Cu addition resulted highly effective in reducing sintering temperature and achieving higher density at lower temperature, while iron doping did not lead to significant improvement with respect to the undoped Mn-Co sample.

The measurement of thermal expansion of the sintered pellets indicated a direct relation between Co substitution and CTE, which decreased with Fe content and was increased by Cu doping. The sample substituted with both Cu and Fe revealed a combined effect on CTE, ranged between that of Fe or Cu doped sample. Similar influence of the composition was observed also on electrical conductivity, lowered by Fe doping and

greatly enhanced by Cu addition, with the mixed Cu-Fe-Mn-Co sample behaving coherently. Substitution of Co with Fe and Cu to obtain a Fe-Cu doped Mn-Co spinel proved therefore as a versatile approach to enhance sintering behaviour and electrical conductivity while retaining thermal expansion compatibility with ferritic stainless steels. This suggests that a multiple doping approach can represent an effective strategy to design cobaltite materials properly tailored on the application.

5. Acknowledgments

This work is supported by the FCH JU within the project SCORED 2:0 under contract. 325331. The authors wish to thank Dr. Claudia Paoletti for the technical support and useful discussions.

Bibliography

- [1] W.Z. Zhu, S.C. Deevi, Development of interconnect materials for solid oxide fuel cells, *Mater. Sci. Eng. A*. 348 (2003) 227–243. doi:10.1016/S0921-5093(02)00736-0.
- [2] K. Hilpert, Chromium Vapor Species over Solid Oxide Fuel Cell Interconnect Materials and Their Potential for Degradation Processes, *J. Electrochem. Soc.* 143 (1996) 3642. doi:10.1149/1.1837264.
- [3] N. Shaigan, W. Qu, D.G. Ivey, W. Chen, A review of recent progress in coatings, surface modifications and alloy developments for solid oxide fuel cell ferritic stainless steel interconnects, *J. Power Sources*. 195 (2010) 1529–1542. doi:10.1016/j.jpowsour.2009.09.069.
- [4] J. Wu, X. Liu, Recent Development of SOFC Metallic Interconnect, *J. Mater. Sci. Technol.* 26 (2010) 293–305. doi:10.1016/S1005-0302(10)60049-7.
- [5] M.Y. Yoon, E.J. Lee, R.H. Song, H.J. Hwang, Preparation and properties of a MnCo_2O_4 for ceramic interconnect of solid oxide fuel cell via glycine nitrate process, *Met. Mater. Int.* 17 (2011) 1039–1043. doi:10.1007/s12540-011-6025-5.
- [6] Z. Yang, G.G. Xia, G.D. Maupin, J.W. Stevenson, Conductive protection layers on oxidation resistant alloys for SOFC interconnect applications, *Surf. Coatings Technol.* 201 (2006) 4476–4483. doi:10.1016/j.surfcoat.2006.08.082.
- [7] X. Montero, F. Tietz, D. Sebold, H.P. Buchkremer, a. Ringuede, M. Cassir, a. Laresgoiti, I. Villarreal, $\text{MnCo}_{1.9}\text{Fe}_{0.1}\text{O}_4$ spinel protection layer on commercial ferritic steels for interconnect applications in solid oxide fuel cells, *J. Power Sources*. 184 (2008) 172–179. doi:10.1016/j.jpowsour.2008.05.081.

- [8] B.-K. Park, J.-W. Lee, S.-B. Lee, T.-H. Lim, S.-J. Park, C.-O. Park, R.-H. Song, Cu- and Ni-doped $\text{Mn}_{1.5}\text{Co}_{1.5}\text{O}_4$ spinel coatings on metallic interconnects for solid oxide fuel cells, *Int. J. Hydrogen Energy*. 38 (2013) 12043–12050. doi:10.1016/j.ijhydene.2013.07.025.
- [9] Y. Xu, Z. Wen, S. Wang, T. Wen, Cu doped Mn–Co spinel protective coating on ferritic stainless steels for SOFC interconnect applications, *Solid State Ionics*. 192 (2011) 561–564. doi:10.1016/j.ssi.2010.05.052.
- [10] K. Wang, Y. Liu, J.W. Fergus, Interactions between SOFC interconnect coating materials and chromia, *J. Am. Ceram. Soc.* 94 (2011) 4490–4495. doi:10.1111/j.1551-2916.2011.04749.x.
- [11] Y. Liu, J.W. Fergus, K. Wang, C. Dela Cruz, Crystal Structure, Chemical Stabilities and Electrical Conductivity of Fe-Doped Manganese Cobalt Spinel Oxides for SOFC Interconnect Coatings, *J. Electrochem. Soc.* 160 (2013) F1316–F1321. doi:10.1149/2.114311jes.
- [12] Z. Yang, G.-G. Xia, X.-H. Li, J.W. Stevenson, $(\text{Mn},\text{Co})_3\text{O}_4$ spinel coatings on ferritic stainless steels for SOFC interconnect applications, *Int. J. Hydrogen Energy*. 32 (2007) 3648–3654. doi:10.1016/j.ijhydene.2006.08.048.
- [13] A. Petric, H. Ling, Electrical Conductivity and Thermal Expansion of Spinel at Elevated Temperatures, *J. Am. Ceram. Soc.* 90 (2007) 1515–1520. doi:10.1111/j.1551-2916.2007.01522.x.
- [14] G. Chen, X. Xin, T. Luo, L. Liu, Y. Zhou, C. Yuan, C. Lin, Z. Zhan, S. Wang, $\text{Mn}_{1.4}\text{Co}_{1.4}\text{Cu}_{0.2}\text{O}_4$ spinel protective coating on ferritic stainless steels for solid oxide fuel cell interconnect applications, *J. Power Sources*. 278 (2015) 230–234. doi:10.1016/j.jpowsour.2014.12.070.

412 [15] A. Masi, M. Bellusci, S.J. McPhail, F. Padella, P. Reale, J. Hong, R.
 413 Steinberger-Wilckens, M. Carlini, Cu-Mn-Co oxides as protective materials in SOFC
 414 technology: The effect of chemical composition on mechanochemical synthesis,
 415 sintering behaviour, thermal expansion and electrical conductivity, *J. Eur. Ceram. Soc.*
 416 37 (2017) 661–669. doi:10.1016/j.jeurceramsoc.2016.09.025.

417 [16] Y. Liu, J.W. Fergus, C. Dela Cruz, Electrical properties, cation distributions, and
 418 thermal expansion of manganese cobalt chromite spinel oxides, *J. Am. Ceram. Soc.* 96
 419 (2013) 1841–1846. doi:10.1111/jace.12254.

420 [17] J. Xiao, W. Zhang, C. Xiong, B. Chi, J. Pu, L. Jian, Oxidation of
 421 MnCu_{0.5}Co_{1.5}O₄ spinel coated SUS430 alloy interconnect in anode and cathode
 422 atmospheres for intermediate temperature solid oxide fuel cell, *Int. J. Hydrogen Energy.*
 423 40 (2015) 1868–1876. doi:10.1016/j.ijhydene.2014.11.124.

424 [18] P. Baláž, M. Achimovičová, M. Baláž, P. Bilík, Z. Cherkezova-Zheleva, J.M.
 425 Criado, F. Delogu, E. Dutková, E. Gaffet, F.J. Gotor, R. Kumar, I. Mitov, T. Rojac, M.
 426 Senna, A. Streletskii, K. Wieczorek-Ciurowa, Hallmarks of mechanochemistry: from
 427 nanoparticles to technology, *Chem. Soc. Rev.* 42 (2013) 7571. doi:10.1039/c3cs35468g.

428 [19] A. Masi, M. Bellusci, M. Carlini, S.J. McPhail, F. Padella, P. Reale,
 429 Mechanochemical Processing of Mn and Co Oxides: An Alternative Way to Synthesize
 430 Mixed Spinel for Protective Coating, *J. Am. Ceram. Soc.* 99 (2016) 308–314.
 431 doi:10.1111/jace.13863.

432 [20] ICPDS.ICDD, -, PCPDF-WIN Version 2.01. (1998).

433 [21] S. Brunauer, P.H. Emmett, E. Teller, Adsorption of Gases in Multimolecular
 434 Layers, *J. Am. Chem. Soc.* 60 (1938) 309–319. doi:10.1021/ja01269a023.

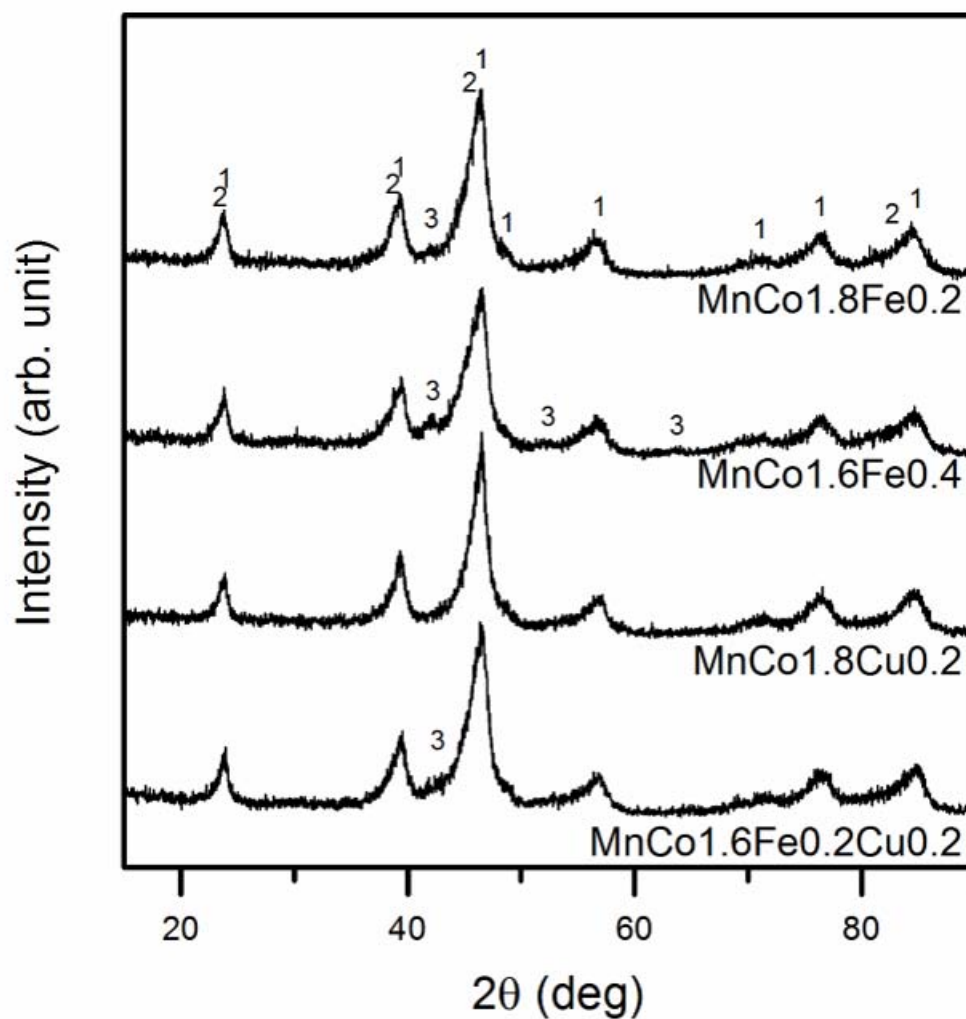
- 435 [22] L.J. van der Pauw, A method of measuring the resistivity and Hall coefficient on
436 lamellae of arbitrary shape, Philips Tech. Rev. 20 (1958) 220–224.
- 437 [23] B. Gillot, DTG Curves of Selective Oxidation of Submicrometer Mixed Valency
438 Spinel: Data Table for the Oxidation Temperature of Transition Metals and Its Relation
439 to the Cation-Oxygen Distance, J. Solid State Chem. 113 (1994) 163–167.
440 doi:10.1006/jssc.1994.1355.
- 441 [24] E. Aukrust, A. Muan, Phase Relations in the System Cobalt Oxide-Manganese
442 Oxide in Air, J. Am. Ceram. Soc. 46 (1963) 511–511. doi:10.1111/j.1151-
443 2916.1963.tb13790.x.
- 444 [25] L. a. Zabdyr, O.B. Fabrichnaya, Phase equilibria in the cobalt oxide-copper
445 oxide system, J. Phase Equilibria. 23 (2002) 149–155. doi:10.1361/1054971023604161.
- 446 [26] R.D. Shannon, Revised effective ionic radii and systematic studies of
447 interatomic distances in halides and chalcogenides, Acta Crystallogr. Sect. A. 32 (1976)
448 751–767. doi:10.1107/S0567739476001551.
- 449 [27] Z. Yang, K.S. Weil, D.M. Paxton, J.W. Stevenson, Selection and Evaluation of
450 Heat-Resistant Alloys for SOFC Interconnect Applications, J. Electrochem. Soc. 150
451 (2003) A1188. doi:10.1149/1.1595659.
- 452 [28] G. Bayer, Thermal expansion of oxide compounds with spinel structure,
453 Thermochim. Acta. 3 (1972) 421–426. doi:10.1016/0040-6031(72)85001-9.
- 454 [29] H. Bordeneuve, C. Tenailleau, S. Guillemet-Fritsch, R. Smith, E. Suard, A.
455 Rousset, Structural variations and cation distributions in $\text{Mn}_{3-x}\text{Co}_x\text{O}_4$ ($0 \leq x \leq 3$) dense
456 ceramics using neutron diffraction data, Solid State Sci. 12 (2010) 379–386.
457 doi:10.1016/j.solidstatesciences.2009.11.018.

458 [30] P. a. Wright, S. Natarajan, J.M. Thomas, P.L. Gai-Boyes, Mixed-metal
459 amorphous and spinel phase oxidation catalysts: characterization by x-ray diffraction, x-
460 ray absorption, electron microscopy, and catalytic studies of systems containing copper,
461 cobalt, and manganese, Chem. Mater. 4 (1992) 1053–1065. doi:10.1021/cm00023a024.

462 [31] E. Elbadraoui, Cation distribution and mechanism of electrical conduction in
463 nickel-copper manganite spinels, Solid State Ionics. 93 (1997) 219–225.
464 doi:10.1016/S0167-2738(96)00559-0.

465

466



468

469 *Fig. 1. X-ray powder diffraction patterns of the different samples after 10h of milling;*

470 *1) Co_3O_4 2) MnCo_2O_4 3) Fe_2O_3 reflections.*

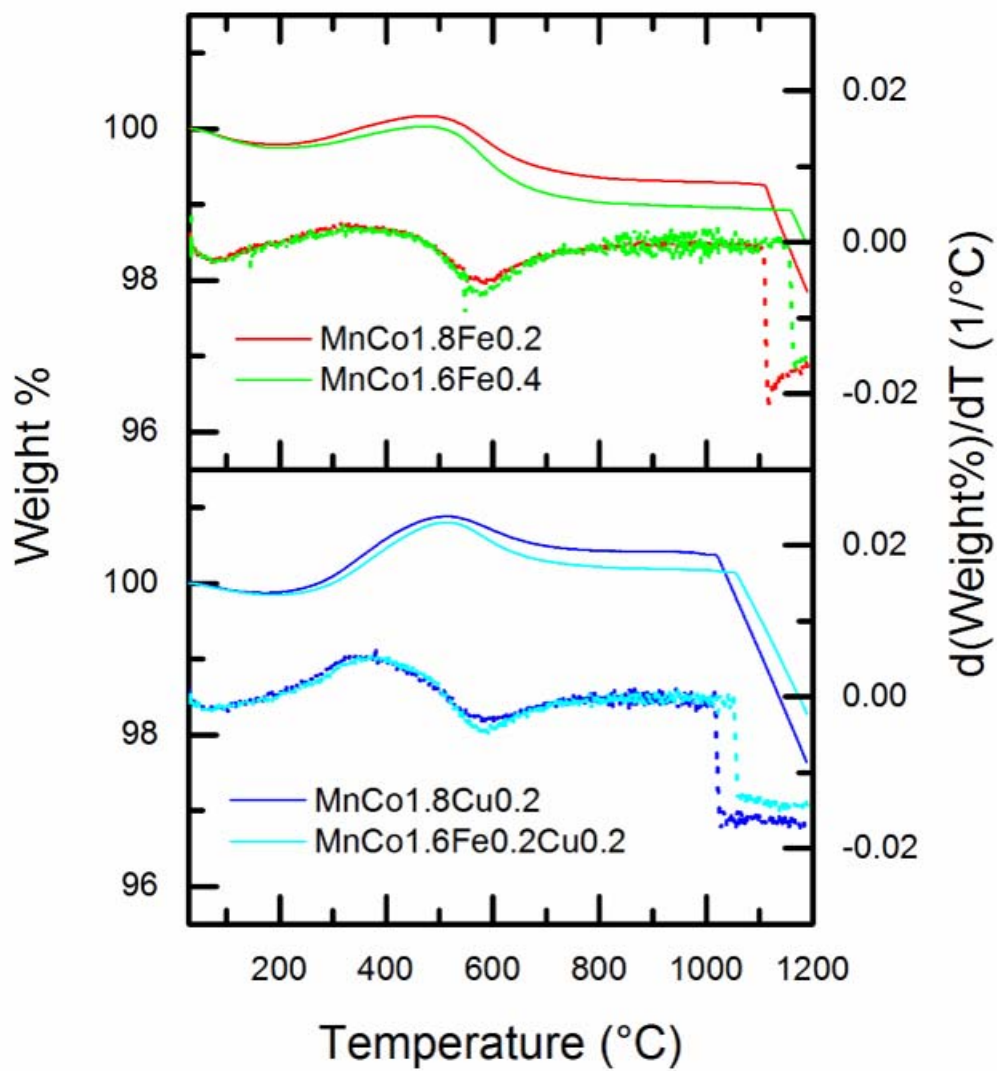


Fig. 2. Thermogravimetric curves as a function of temperature for the different samples; solid lines represent weight% change, dotted lines the derivative of weight% versus temperature.

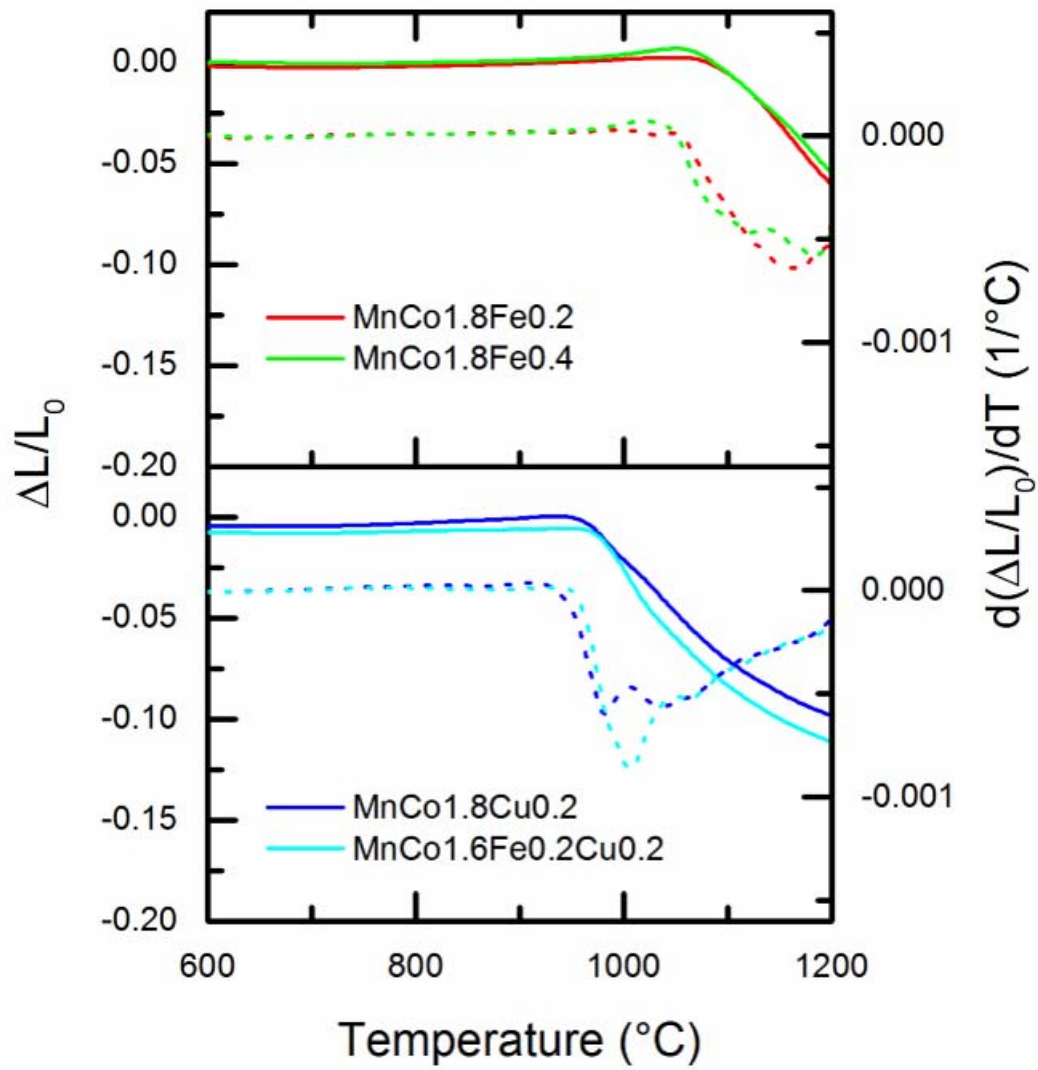
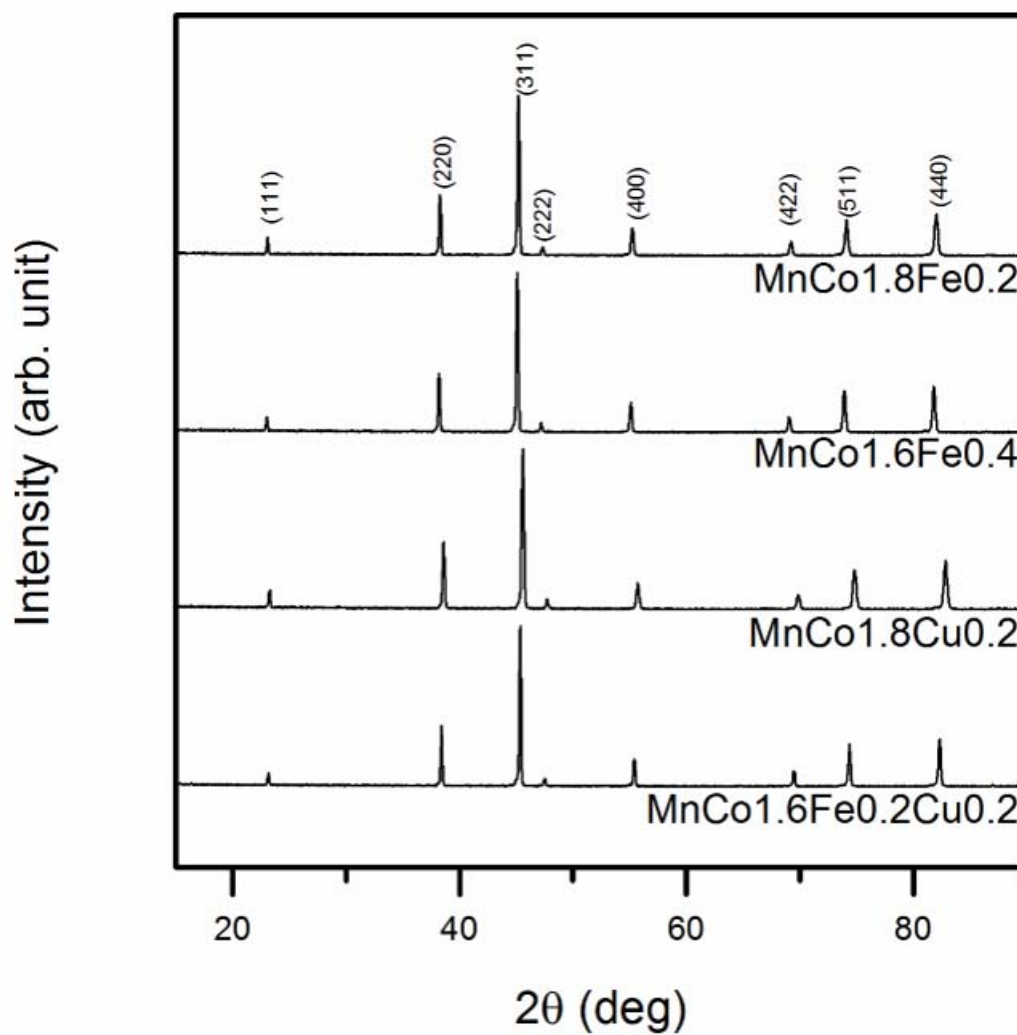


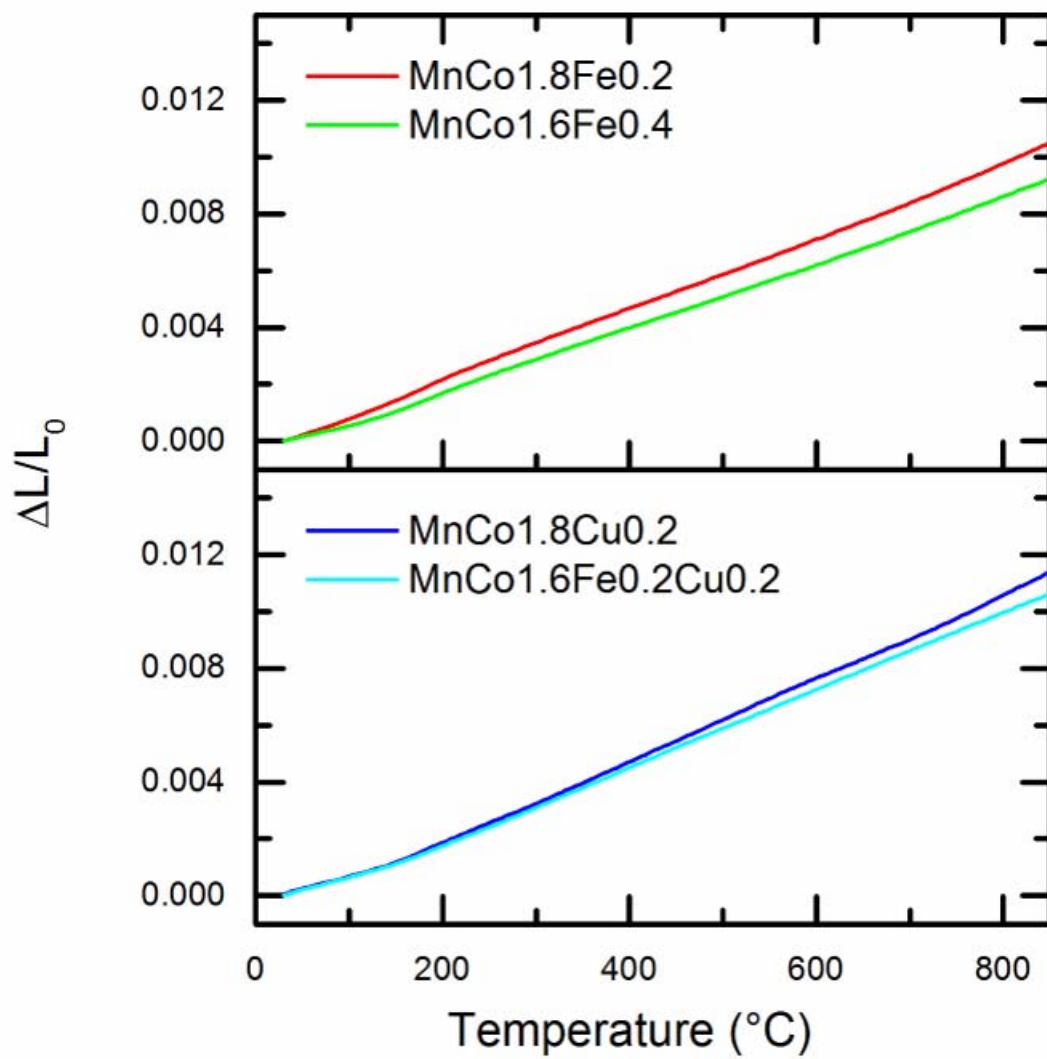
Fig. 3. Dilatometric curves as a function of temperature of the different samples; solid lines represent the length change, dashed lines the derivative of the length change versus temperature.



479

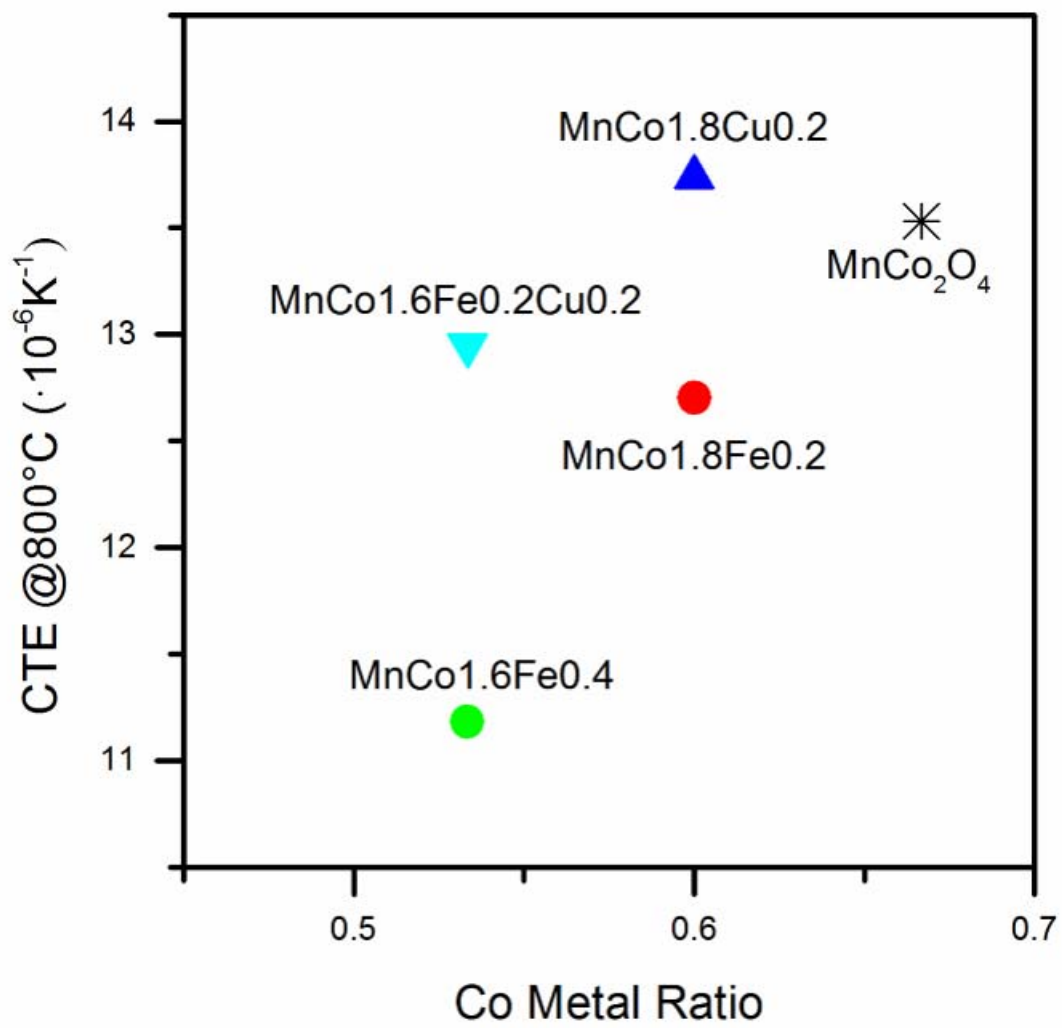
480 *Fig. 4. X-ray powder diffraction patterns of the samples after sintering treatment;*

481 *specified reflections are ascribable to a cubic spinel phase.*



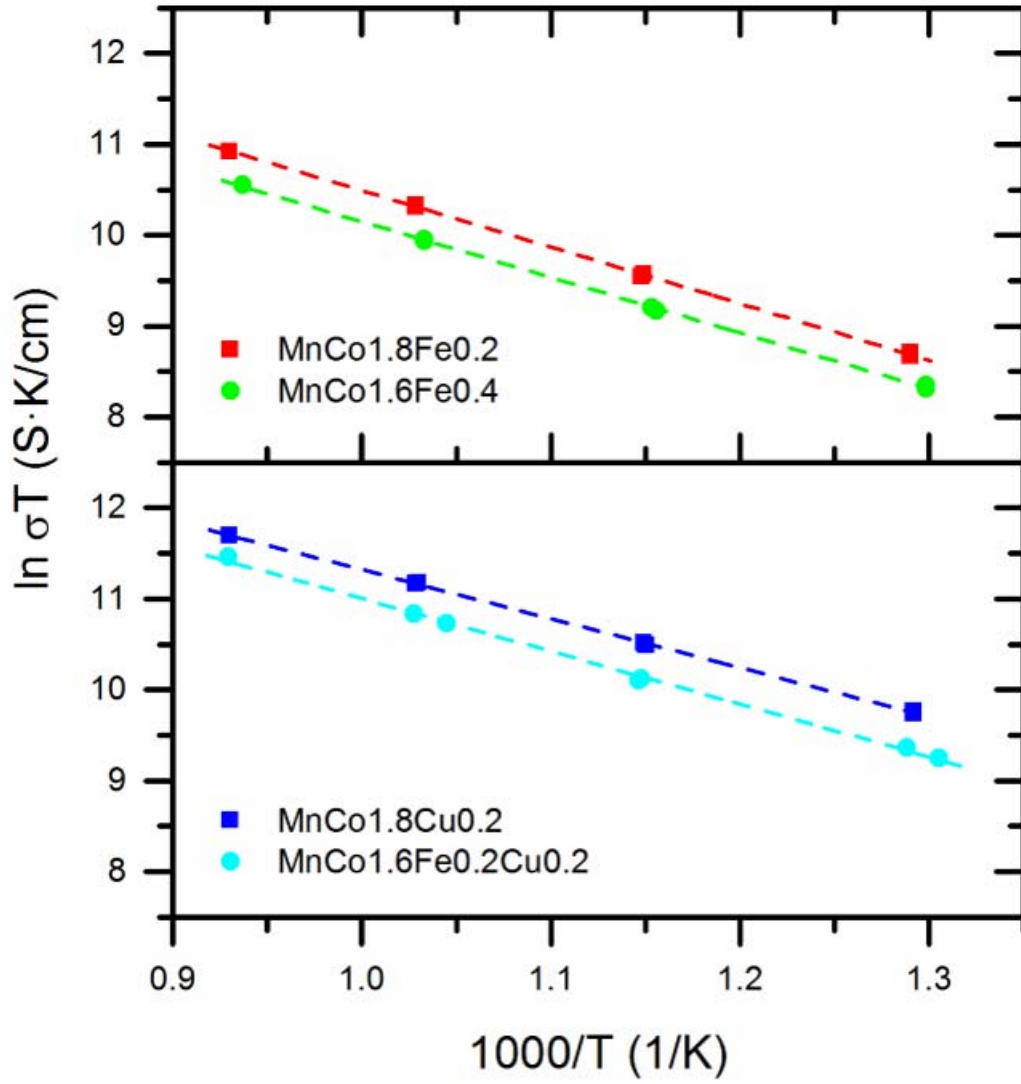
482

483 *Fig. 5. Thermal expansion curves of the sintered samples.*



484

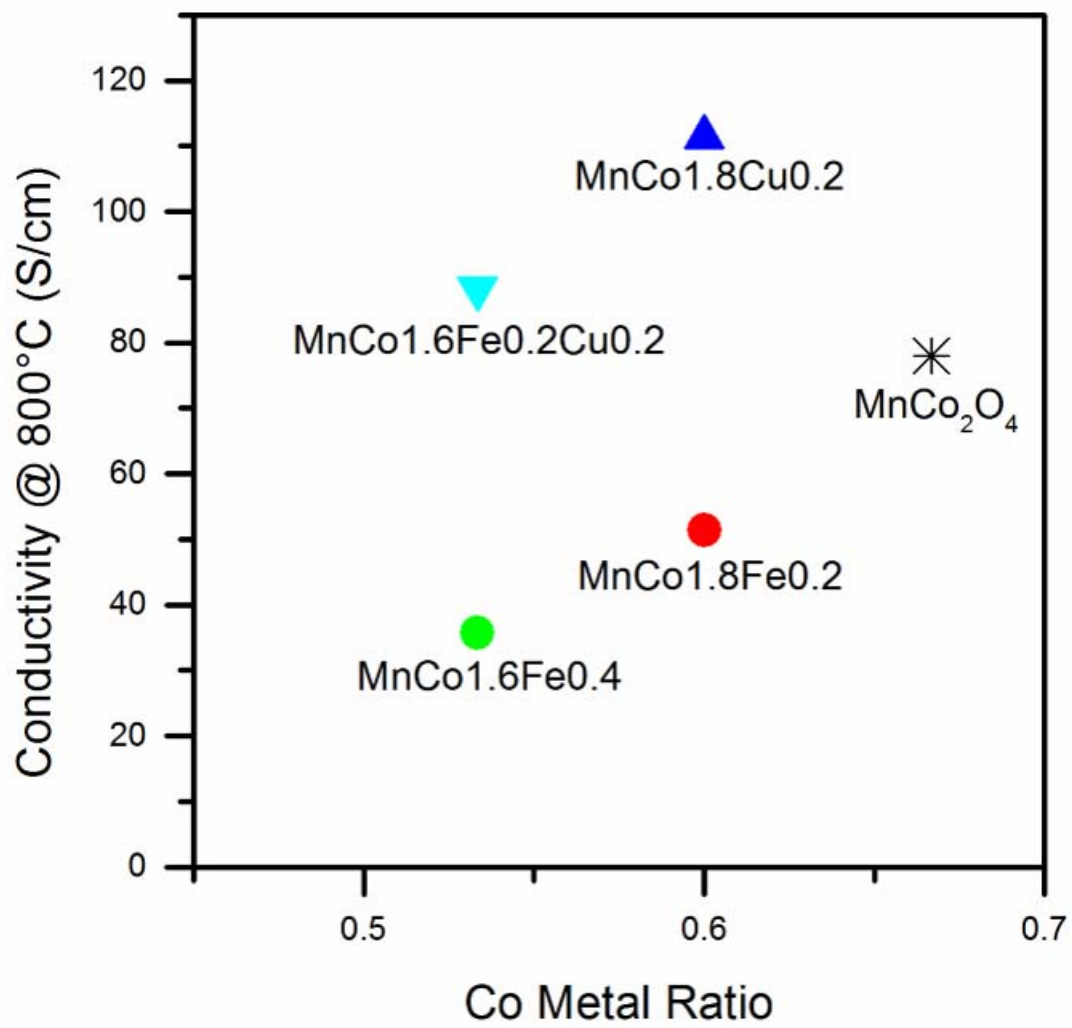
485 *Fig. 6. Coefficient of thermal expansion calculated at 800°C as a function of the Cobalt*
 486 *substitution in comparison with the undoped material (as reported in [15]).*



487

488 *Fig. 7: Arrhenius plots of electrical conductivity measured (dots) for the different*

489 *samples and linear fits of the experimental points (dashed lines).*



490

491 *Fig. 8. Conductivity values measured at 800°C as a function of the Cobalt substitution*
 492 *in comparison with the undoped material (as reported in [15]).*

493

494

Tables

Table 1: Sample nomenclature and nominal composition.

Sample name	Atomic ratio				Nominal composition
	Mn	Co	Fe	Cu	
MnCo1.8Fe0.2	0.33	0.60	0.07		MnCo _{1.8} Fe _{0.2} O ₄
MnCo1.6Fe0.4	0.33	0.53	0.14		MnCo _{1.6} Fe _{0.4} O ₄
MnCo1.8Cu0.2	0.33	0.60		0.07	MnCo _{1.8} Cu _{0.2} O ₄
MnCo1.6Fe0.2Cu0.2	0.33	0.53	0.07	0.07	MnCo _{1.6} Fe _{0.2} Cu _{0.2} O ₄

Table 2: BET surface area and BET particle size for the 10h HEBM powders.

Sample	BET	l*
	(m ² /g)	(nm)
MnCo1.8Fe0.2	6.0±0.3	182±9
MnCo1.6Fe0.4	6.8±0.3	163±8
MnCo1.8Cu0.2	3.3±0.2	323±20
MnCo1.6Fe0.2Cu0.2	3.8±0.2	287±16

$$*l = \frac{6}{SSA \cdot \rho}$$

Table 3: Sintering thermal treatments.

Sample	Green density (%)	Sintering treatment	Sintered density (%)
MnCo1.8Fe0.2	66±1	4 h @1200°C + 4 h @800°C	92±1
MnCo1.6Fe0.4	66±1	4 h @1200°C + 4 h @800°C	90±1
MnCo1.8Cu0.2	65±1	4 h @1000°C + 4 h @800°C	97±1
MnCo1.6Fe0.2Cu0.2	65±1	4 h @1000°C + 4 h @800°C	95±1

Table 4. Lattice parameter (a) of the cubic spinel cell calculated from XRD patterns of the sintered samples.

Sample	a (Å)
MnCo1.8Fe0.2	8.319(7)
MnCo1.6Fe0.4	8.351(8)
MnCo1.8Cu0.2	8.277(8)
MnCo1.6Fe0.2Cu0.2	8.312(8)

Table 5. Thermal expansion coefficient measured between room temperature and 800°C for the different samples.

Sample	CTE ($\cdot 10^{-6} \text{ K}^{-1}$) [30°-800°]
MnCo1.8Fe0.2	12.7±0.1
MnCo1.6Fe0.4	11.1±0.1
MnCo1.8Cu0.2	13.7±0.1
MnCo1.6Fe0.2Cu0.2	12.9±0.1

512 *Table 6. Activation energy calculated from the Arrhenius plot of 10 hours milled*
 513 *samples.*

Sample	Ea (eV)
MnCo1.8Fe0.2	0.54±0.03
MnCo1.6Fe0.4	0.53±0.03
MnCo1.8Cu0.2	0.46±0.03
MnCo1.6Fe0.2Cu0.2	0.50±0.03

514